ACS APPLIED NANO MATERIALS

Article

Cite This: ACS Appl. Nano Mater. 2018, 1, 6123−6130

www.acsanm.org

Tailoring Composition and Material Distribution in Multicomponent Cryoaerogels for Application in Photocatalysis

Axel Freytag,[†,‡] Carsten Günnemann,[†,‡] Suraj Naskar,[†,‡] Saher Hamid,[§,‡,⊥] Franziska Lübkemann,[†,‡] Detlef Bahnemann,[§,‡,⊥] and Nadja C. Bigall*[,†,‡]

[†]Institute of Physical Chemistry and Electrochemistry (PCI), [‡]Laboratory of Nano and Quantum Engineering (LNQE), and [§]Institute for Technical Chemistry, Leibniz Universität Hannover, D-30167 Hannover, Germany

[⊥]Laboratory "Photoactive Nanocomposite Materials", Saint-Petersburg State University, Ulyanovskaya str. 1, Peterhof, Saint-Petersburg 198504, Russia

Supporting Information

ABSTRACT: In this article, we demonstrate the fabrication of tailored multicomponent cryoaerogels from colloidal nanoparticles via the cryogelation method. With this method, it is possible to control the amount of components very precisely. Furthermore, the microscopic distribution of the different nanoparticle components in the resulting monolithic structure is shown to be adjustable by simply mixing calculated amounts of colloidal nanoparticle solutions with a suitable surface charge. We focus on titania cryoaerogels due to their potential for optical applications and investigate the properties of synthesized titania-gold cryoaerogels in dependency of the composition. In addition, titania-platinum cryoaerogels were tested for photocatalytic applications such as hydrogen evolution and showed a significant increase in performance and stability compared to their respective colloidal solutions. While showing comparable results for hydrogen evolution with aerogels as reported in literature, the fabrication is much faster and less complex and therefore might enable future industrial application.

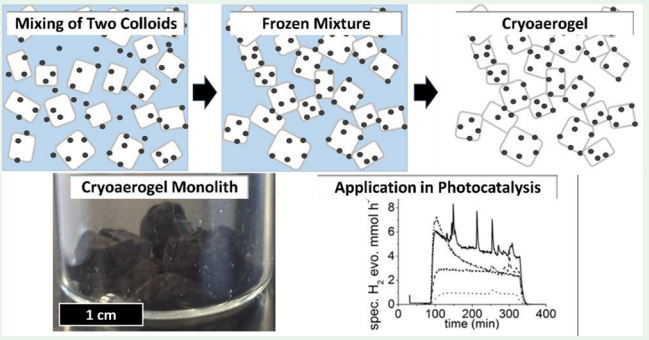

KEYWORDS: *multicomponent, aerogel, photocatalytic hydrogen evolution, cryoaerogelation, colloidal nanoparticles*

INTRODUCTION

Aerogelation is one way to assemble nanoparticles into macroscopic structures. These materials show unique features such as low density and low thermal conductivity, which cannot be obtained by conventional materials.[1,2] Aerogels already found applications as filter material for stardust or as transparent thermal insulation.[3,4] However, the potential of aerogels is still not fully exploited since recently they can be fabricated of colloidal nanoparticles such as (noble) metals and semiconductors as well as metal oxides.[2,5−12] Hence, it is more and more possible to tune aerogels with desired properties by using specific nanoparticles such as photoactive or conductive components as well as catalytic components, which are highly selective.[8,13,14] Combined with the advantages of large specific surface area and large interface area between the components, and therefore shorter path lengths (e.g., in diffusion processes), aerogels are expected to be excellent catalysts and sensors.[15−18] However, there are barely reports on aerogels applied in, for example, industrial catalysis or electronics, which are based on two main reasons. One reason is that the stability (mechanical and thermal) of aerogels has not met the requirements for the aimed applications so far, or, when the requirements were met, the complexity in fabrication made them unsuitable for larger scale application.[13,14,17] The second reason is composite materials (which can overcome the lack of stability) have certain limitations in distribution of the materials and yields that can be used to obtain aerogels.[1,19,20] Recently we reported on a new method of fabricating aerogels entitled the cryoaerogelation method.[21] This procedure allows the employment of different nanoparticles as building blocks for aerogels without prior complex adjustment of the surface chemistry as long as the nanoparticles are dispersed in aqueous solution. Cryoaerogelation is freezing and subsequent freeze-drying used to assembly nanoparticles while retaining their properties. All other gelation methods (i.e., aerogelation by first inducing assembly in liquid environment and subsequent either supercritical or freeze-drying) are very complex and time-consuming. Especially, since in these cases first gelation in liquid by chemical routes must be achieved, such conventional routes always need the development of a specific respective chemical gelation, which can vary drastically for different nanoparticle compositions or surface chemistry. The big

Received: July 31, 2018
Accepted: October 18, 2018
Published: October 26, 2018

Scheme 1. Synthesis Route to Multicomponent Cryoaerogels[a]

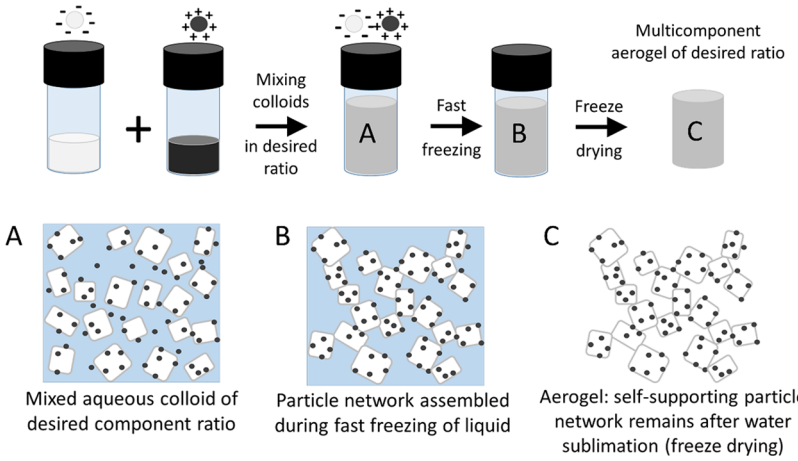

[a](Top) By mixing nanoparticle solutions in the desired composition ratio with subsequent cryoaerogelation, multicomponent aerogels of desired composition ratio can be achieved. (Bottom. A–C) In detail, the nanoparticles distribute (arbitrarily) in a homogeneous way if mixed with opposite surface charges.

advantage of the assembly during the freezing process as described by our route is that it is completely independent of the type, size, and surface chemistry of the nanoparticles. Hence, this method seems promising also for low-cost and large scale aerogel fabrication. However, it needs to be investigated in respect of its potential for multicomponent aerogelation to target the need for more complex multicomponent catalysts for future applications.

In the present work, we demonstrate that by cryoaerogelation we are able to fabricate mixed composite cryoaerogels. The article focuses on the composition tailoring of their microstructure. We show how the method can be utilized and what tools (e.g., zeta potential) can be used. We show that this route has basically no restriction on the inserted components and enables a freely variable composition ratio. This supports catalyst design, for example, for photocatalytic hydrogen evolution or many further applications. In detail, in the present article we show the fabrication of metal-oxide noble-metal aerogel systems. While this route is applicable on various types of material compositions, here, the focus is exemplarily set on titania. We can control the distribution of the components within the aerogel by adjusting the ζ-potential of the employed nanoparticles. Furthermore, we can adjust the ratio of the two components in the resulting monolith by mixing the two nanoparticle solutions in the desired composition ratio prior to cryoaerogelation. We investigate how the optical properties of noble-metal TiO_2 cryoaerogels vary with changing the component ratios. Finally, we show proof-of-principle measurements for hydrogen evolution reaction with TiO_2–Pt cryoaerogels exhibiting 5.1 mmol h^{-1} g^{-1} for 1 wt % Pt content, which are promising results comparable to recent literature values.

RESULTS AND DISCUSSION

We synthesized multicomponent monoliths of titania noble-metal cryoaerogels following the cryoaerogelation method (see also Scheme 1). The fabrication can be achieved by mixing aqueous colloidal solutions, fast freezing this solution (e.g., with liquid nitrogen) and subsequent freeze-drying of the frozen colloids. The resulting monoliths are highly voluminous, porous, and lightweight. While we focus in this work on titania noble-metal systems (Au, Ag, Pt), the series of fabricated material combinations was extended to other metal-oxide noble-metal systems such as hematite noble-metal (Au, Ag, Pt) as well as metal-oxide-hydroxides Pt (see Supporting Information Figure S1). Although they have different macroscopic appearances in color due to varying material and component ratios, the microscopic morphology is for all synthesized cryoaerogels similar. The morphology can be described as interconnected thin sheets, which again are made of assembled nanoparticles. To simplify, the morphology is a 3D structure made of 2D nanoparticle assemblies.

The structure is a result of freezing the aqueous colloidal solution, where the formed ice crystals act as template for the nanoparticles to yield the final cryoaerogel structure. The respective mechanism was described already in our earlier report.[21] It should be mentioned that for pure TiO_2 and hematite systems, the monoliths easily disintegrate and are better described as voluminous powder. The fragile nature of the pure metal oxide system can be explained with low attractive interactions between the particles. While the intraparticle interactions (namely ionic bonding) are quite strong due to close proximity and high difference in electronegativity of the oxygen and metal ions, the interparticle interactions are relatively weak, which is mainly due to the fact that the average atom distances between the neighboring nanoparticles are higher than within the nanoparticles.[22] Furthermore, additional Coulomb forces may occur due to the presence of surfactants binding to the nanoparticle surface (from colloidal synthesis). While being in a colloidal solution, the ligands serve to stabilize the nanoparticle due the surface charge and prevent agglomeration. Out of the aqueous solution, the ζ-potential is of no concern.[23,24] However, humidity at ambient conditions in a highly porous system may still effect the ligands on the particle surface. Therefore, weak Coulomb interactions between the particle surfaces may occur and must be taken into account. We observe improved interconnection after cryoaerogelation between the nanoparticles and an increased self-supportability of the resulting monolithic aerogel assemblies. Additionally, the employment of ligands may lead to cross-linking effects and contribute to the cohesion of the monolith. Besides the stabilizing ligands for

DOI: 10.1021/acsanm.8b01333
ACS Appl. Nano Mater. 2018, 1, 6123–6130

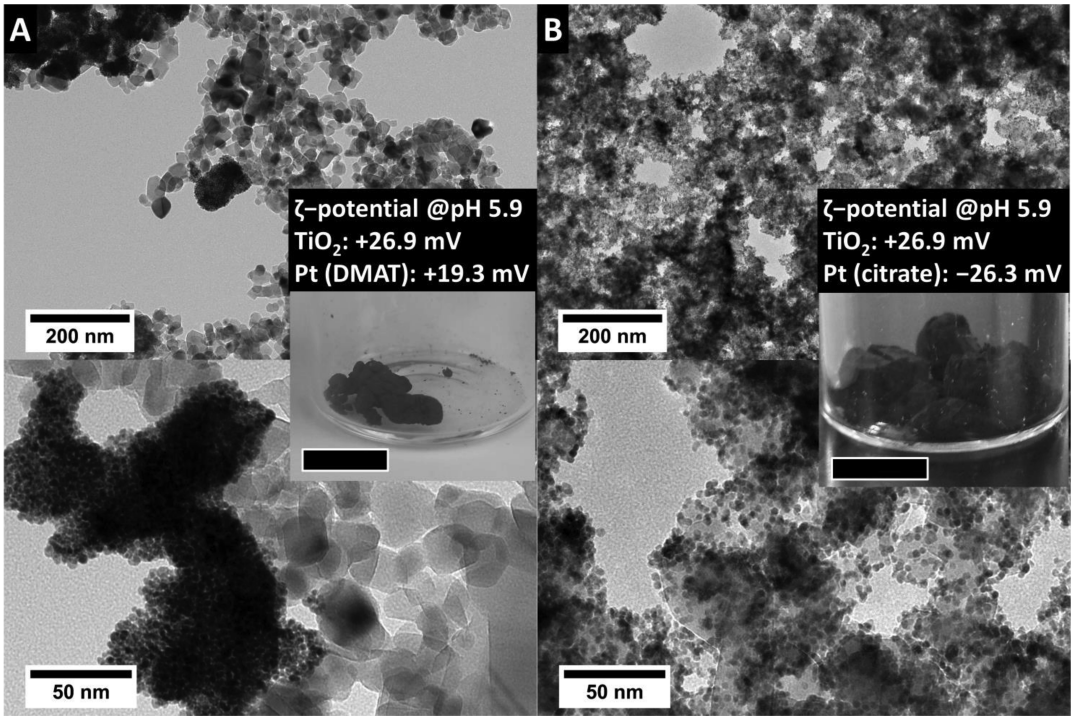

Figure 1. Component distribution of cryogelated aerogels in dependence of the ζ-potential of the employed nanoparticles derived from transmission electron micrographs in two different magnifications (top and bottom, respectively). The left images (A) show a partly segregation of the nanoparticles when employing two nanoparticles of similar ζ-potential (Pt nanoparticles with 2-dimethylaminoethanethiol ligands). The inset shows a photograph of the TiO_2−Pt cryoaerogel (scale bar represents 1 cm). The right images (B) demonstrate a homogeneous component distribution. We assume that attraction of the oppositely charged nanoparticles leads to the homogeneous distribution already in solution prior to cryoaerogelation. The inset shows a photograph of the TiO_2−Pt cryoaerogel (scale bar represents 1 cm).

the noble metal nanocrystals (namely, citrate and dimethylaminoethanethiole (DMAT) ligands remaining partially after excessive ultrafiltration), no further ligands were present to achieve the monolithic cryoaerogels, to warrant the accessibility of the nanoparticles in the superstructures. However, for different purposes than reported here, it might also be a possibility to add higher amounts of ligands to create more cross-linking interactions like, for example, intercalation of steric ligands on purpose to obtain more stable monoliths.

Raising the metal content or applying heat treatment (for example 150 °C) to these cryoaerogels leads to increased stability (i.e., less brittleness) of the metal oxide monoliths, which can be explained by two reasons. First, the heat treatment can decrease interparticle distances and therefore enhance the mechanical and thermal stability.[22] However, care should be taken with the annealing parameters since treatment at higher temperatures such as 400 °C resulted in strong shrinkage or collapse of our metal oxide hydroxide cryoaerogels. Second, by adding the significantly smaller noble metal nanoparticles, voids within the assembled nanoparticles can be filled improving the contact between them, which also results in better stability.

We observed that the ζ-potentials of the nanoparticle species from solution influence their distribution within the colloid and therefore in the subsequent aerogel. It is a well-known method to stabilize nanoparticles in colloidal solution with a ζ-potential of the same charge, creating repulsion forces between the particles and preventing agglomeration. This repulsion also takes place when mixing two different colloids and prevents attachments of particles on each other. However, upon freezing such a colloidal solution consisting of two different nanoparticle species with all similar surface charges and subsequently freeze-drying it, we found a local segregation in the resulting cryoaerogel, as can be derived from Figure 1A for the example of a TiO_2−Pt cryoaerogel.

In the case of similar ζ-potentials for both compounds, we found local islands of Pt in the size of several hundred nanometers for 50 wt % and many TiO_2 nanoparticles with no Pt attached. The TiO_2 cryoaerogel with 1 wt % Pt shows less inhomogeneous distributions, meaning regions of TiO_2 nanoparticles with no Pt nanoparticles in the surrounding area and local areas with a high concentration of Pt nanoparticles in the size of 50 nm. Since we confirmed by DLS (see Figures S3−S6) that by simply mixing the two types of nanoparticles of similar ζ-potentials no agglomeration takes place, we attribute the compound segregation in case of the cryoaerogels to the higher mobility of the smaller Pt nanoparticle being immobilized after the TiO_2 nanoparticles.

Instead, if for example via ligand exchange, the ζ-potential of the employed nanoparticle is changed to opposite charges, we observe for the same TiO_2−Pt nanoparticle mixtures a homogeneous material distribution in the resulting cryoaerogels (see Figure 1B). The Pt nanoparticles are found to be attached to the TiO_2 nanoparticles in this case, in a very homogeneous way. We assume the attachment occurs already in solution, shortly after mixing, due to the opposite surface charges. However, this assumption is difficult to prove since light scattering based techniques such as DLS are unsuitable upon colloid mixtures of such different sizes. We investigated the colloidal solution by transmission electron microscopy (TEM) immediately after mixing the solutions (see Figure S2) as well as after cryogelation (Figure 1). The distribution of the

DOI: 10.1021/acsanm.8b01333
ACS Appl. Nano Mater. 2018, 1, 6123−6130

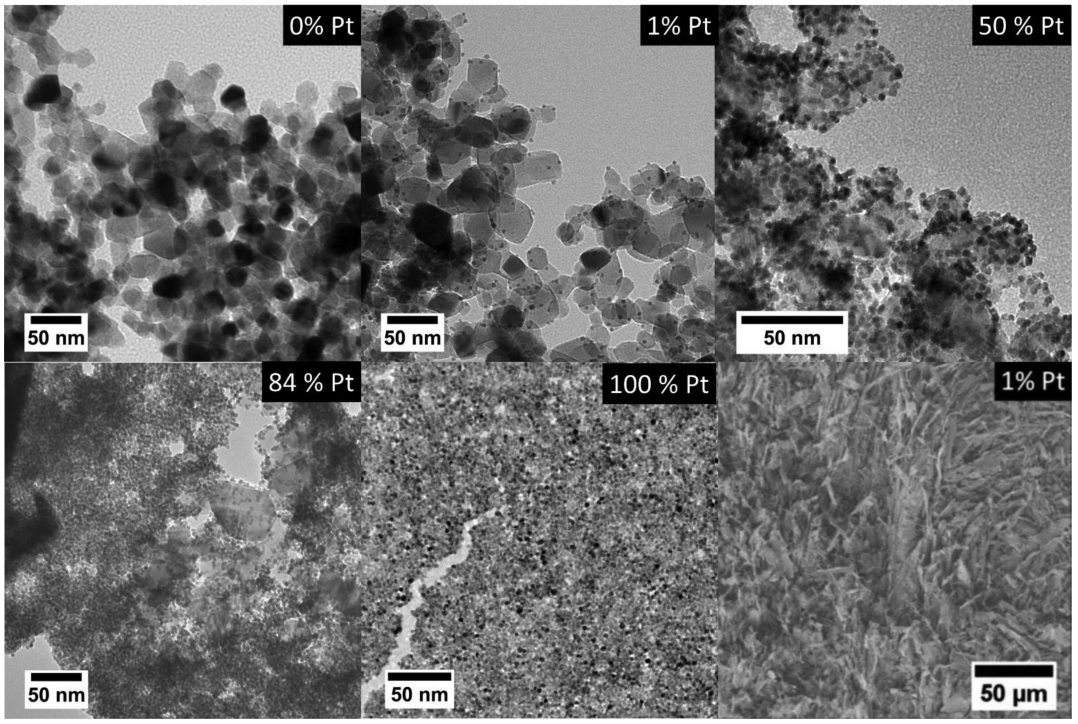

Figure 2. TEM characterization of TiO_2 cryoaerogels with increasing platinum loading ranging from 0 to 100% Pt yield. The surface potential was positive for TiO_2 and negative for Pt nanoparticles ensuring homogeneous distribution. The lower right image shows a SEM image to demonstrate the morphology in the micrometer size.

particles was found to be homogeneous at both states of the synthesis, meaning every TiO_2 or hematite nanoparticle has noble metal nanoparticles as direct neighbors in nearly all cases (only exception: employment of already agglomerated Ag nanoparticles in the colloidal solution, see Figure S7, such cryoaerogels also exhibit a very low surface area see Figure S8). However, the attachment of the noble metal to the metal oxide nanoparticles when the TEM sample was prepared from solution could also be a consequence of the TEM grid preparation itself, that is, caused by drying effects.

By adjusting the ζ-potential through ligand exchange, we always achieved the intended (homogeneous or heterogeneous) component distribution, that is, both for the TiO_2 noble-metal and for the hematite noble-metal systems. The homogeneous compound distribution on a larger scale was proven by energy-dispersive X-ray spectroscopy (EDX) mappings during scanning electron microscopy (SEM) imaging (see SI Figure S4).

In a different set of experiments, we found that the composition of cryogelated aerogels can be freely varied by simply mixing the calculated amounts of colloidal nanoparticle solution. We prepared TiO_2 cryoaerogels with different loadings of Pt, Ag, and Au. For the TiO_2–Pt system, besides 0 and 100 wt % Pt nanoparticles, we also selected the ideal metal loading for water splitting applications of 1 wt % (as shown by Kaise[25]) as well as equivalent mass (50 wt %) and equivalent volume (84 wt %) of the employed nanoparticle fractions. Between 1% and 50% and even much higher ratios, every desired composition can be realized. However, since we did not expect any interesting effect for this composition range, we chose these three compositions for the present publication to demonstrate how broadly the composition range can be chosen by our technique. The ζ-potential was negative for the Pt and positive for TiO_2, which is necessary to obtain a homogeneous distribution of the components as discussed above. Characterization with transmission electron microscopy shows the distribution of the nanoparticles for all compositions (see Figure 2). In these cryoaerogels, nearly all Pt nanoparticles were directly attached to the TiO_2 surface. The crystal structures of the as-synthesized mixed Pt-TiO_2, Au-TiO_2, and Ag-TiO_2 were determined with X-ray diffraction and compared to the starting compound (see SI Figures S9–S11). We observed no change in the crystal phases throughout the fabrication.

Spectroscopic characterization of cryoaerogel films from TiO_2–Ag (see Figure S7) as well as TiO_2–Au (see Figure 3) systems reveals that the properties of the employed single components (namely the occurrence of localized surface plasmon resonances LSPRs) could be transferred to the macroscopic multi component cryoaerogels. The optical spectrum of the final mixed monolith is significantly influenced

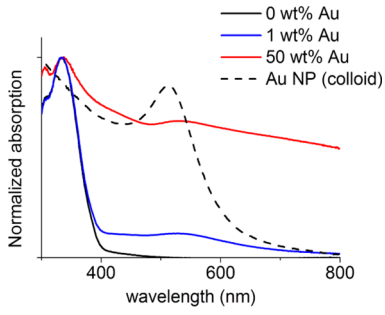

Figure 3. Normalized absorption spectra of mixed composite cryogelated aerogel films for the systems TiO_2–Au with composition ratios of 0 wt % (pure TiO_2 cryoaerogel), 1 wt % Au, and 50 wt % Au. Black dotted lines show the spectra of the respective particle colloids.

DOI: 10.1021/acsanm.8b01333
ACS Appl. Nano Mater. 2018, 1, 6123–6130

by the optical properties of both components. Generally, all spectra show absorption maxima at 350 nm, which corresponds to the band gap of TiO_2 of a nanoparticular size. The spectra of the systems of TiO_2–Au with 1 and 50 wt % Au show an extinction maximum around 540 nm. The bathochromatic shift of the LSPR of 15 nm compared to the colloidal solution can be explained by the change of the dielectric function caused by a changed environment (see Figure 3). The broadening of the maximum is presumably caused by interplasmon interactions caused by the various different interparticle distances in the assembled superstructure.[26−29] In conclusion, the optical spectra of the mixed cryoaerogel films differ significantly compared to that of the pure TiO_2 cryoaerogel. This means that the optical properties of the resulting monolith can be influenced to a certain degree by adjusting the ratio of both compounds.

Because of their good surface accessibility in combination with the ability of facile separation from the reaction mixture, gels are of interest for solution-based catalysis. In the present case, the fabricated cryoaerogel monoliths from mixed components are of potential interest for applications like, for example, in photocatalytic hydrogen evolution, due to their exact tunability of the compound ratios. The role of platinum for the photocatalytic hydrogen production has been studied in detail before.[30] Conduction band electrons photogenerated in TiO_2 are readily transferred to the Pt-islands, thus preventing the undesired electron/hole recombination. Subsequently, that is in the catalytic reaction step, these electrons are reacting with protons at the surface of the Pt particles forming surface adsorbed hydrogen atoms, which then combine to form the observed hydrogen gas. In the parallel reaction of the holes, the sacrificial reagent methanol is oxidized initially to α-hydroxymethyl radicals, which then inject an electron most likely directly into the Pt deposit to form formaldehyde (current-doubling effect). Once the sacrificial reagent has been totally oxidized to CO_2, the H_2 formation ceases.[30]

For proof-of-principle, we therefore tested TiO_2–Pt systems with varying Pt amounts of 1, 50, and 84 wt % for their capability of hydrogen evolution from water under illumination with a 1000 W xenon lamp under assistance of methanol as hole scavenger. We choose this reaction since it is well investigated and enables comparison of the fabricated cryoaerogels to hydrogelated aerogels.[13] First we varied the amount of Pt in the system TiO_2–Pt (see Figure 4). The highest hydrogen evolution could be observed for systems with 1 wt % Pt as already reported previously.[25] This is readily understood since, as the Pt-content is increased, the amount of light that can be absorbed by the photocatalyst decreases, thus limiting the possible maximum photocatalytic efficiency since any light absorbed by Pt is "lost" for the photocatalytic reaction.

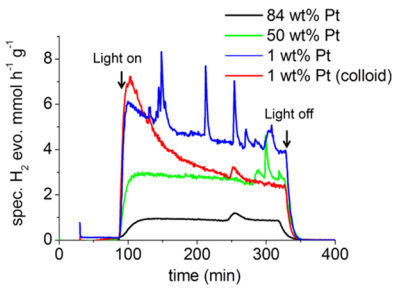

Figure 4. Specific hydrogen evolution for TiO_2 Pt cryoaerogels with varying Pt content of 1, 50, and 84 wt % and the colloidal solution of TiO_2 with 1 wt % Pt to compare the effect of the cryoaerogelation with the colloidal solution.

We measured the average specific hydrogen evolution to be 5.1 mmol h^{-1} g^{-1} for 1 wt % Pt, 3.0 mmol h^{-1} g^{-1} for 50 wt % Pt, and 1.0 mmol h^{-1} g^{-1} for 84 wt % Pt and compared to the data of a nongelated mixed TiO_2–Pt colloid (with 1 wt % Pt). Da Silva et al.[13] achieved for a hydrogelated aerogel system with similar compound compositions 6.9 mmol h^{-1} g^{-1} but with a 400 W Hg lamp. This means, by cryoaerogelation, comparable hydrogen evolution rates can be achieved to those of aerogels from conventional gelation routes, yet with a faster and less complex fabrication method.

The average specific hydrogen evolution rate was measured to be 3.1 mmol h^{-1} g^{-1} for the colloidal solution with 1 wt % Pt. We attribute the ability of producing hydrogen within the colloidal nanoparticle solution to the adsorption of the oppositely charged particles. It presumably takes place as soon as the two colloidal solutions are mixed because of the opposite zeta potential of the Pt (which we measured to be −50.3 mV ± 1.5 mV @ pH 7) and TiO_2 nanoparticles (26.9 mV ± 0.3 mV @ pH 7) as discussed above. The average performance for hydrogen evolution after cryoaerogelation (integrated over the illumination time of 240 min) is increased by around 60% for cryoaerogels in comparison to the nanoparticle mixture. In addition, the performance over time becomes more stable compared to the colloidal system. This is probably due to the immobilization of the particles into stable small units when roughly dispersing the cryoaerogels in the reaction mixture (see Discussion above), while the colloidal solution is only loosely bound through surface charges. The surface charge, especially from TiO_2, can locally change during the hydrogen formation reaction[25] leading to attaching and detaching of Pt nanoparticles onto and from the TiO_2 nanoparticles, which leads to a decrease of the efficiency over time. For the cryoaerogelated system, we also observe spikes during the measurement. These peaks, which can be seen in Figure 4, are not caused by any experimental noise; however, they are signs of real rate changes, which we explain as follows. We attribute these spikes to the nanoporous structure of the cryogel. Produced hydrogen can be captured in these porous structures and is promptly released when reaching certain volumes. With further experiments, we determined the total surface of the produced titania noble-metal cryoaerogels to be ranging from 40 to 47 m^2 g^{-1} for 1% noble metal content and 5 to 7.8 m^2 g^{-1} for 50% noble metal content. The total pore volume is in the range of 10^{-2} cm^3 g^{-1} for 1% to around 10^{-3} cm^3 g^{-1} for 50% noble metal content, respectively. Here, we can assume a correlation of the total pore volume and the volume of hydrogen that represents the spikes in Figure 4, both being in the same magnitude.

CONCLUSION

In summary, fabricating composite aerogels via cryoaerogelation of nanoparticle solutions offers a high degree of control over the properties of the resulting monoliths. Material compositions can be freely varied and particle distributions within the gels adjusted. By this variation also the optical properties can be influenced. We found in our experiments that the ζ-potential, material, and the composition ratio of the employed nanoparticles are the crucial parameters for tuning the aerogel properties. This high degree of control can, for

DOI: 10.1021/acsanm.8b01333
ACS Appl. Nano Mater. 2018, 1, 6123−6130

example, be exploited to fabricate tailored multicomponent cryoaerogels for (photo)catalysis. Further applications such as optical or electronical sensing can be determined. We could demonstrate with our cryoaerogel comparable hydrogen evolution rates compared to the best literature values for conventionally hydrogelated aerogels and show a significant increase of performance and stability compared to that of the respective colloidal solutions. Since the cryoaerogelation synthesis is less complex as well as faster in comparison to previous gelation methods, our results might make the cryoaerogelation interesting for creating a new generation of tailored multicomponent photocatalysts, catalysts, and sensors.

MATERIALS AND METHODS

Materials. Dihydrogen tetrachloroaureate hexahydrate (99.99%), dihydrogen tetrachloroplatinate (IV) hexahydrate (99.95%), trisodium citrate (reagent grade), and sodium hydroxide (reagent grade) were purchased from ABCR. Sodium borohydrate (99.9%) was purchased from Fluka. Silver nitrate (>99.0%) and iron(III) chloride hexahydrate (99%) were purchased from Alfa Aesar. 2-Dimethylaminoethanethiol (DMAT, >99%), TiO_2 nanoparticles (P25), $MnCl_2{\cdot}4H2O$, (>99.0%), $CoCl_2{\cdot}6H2O$ (>99.0%), $NiCl_2{\cdot}6H_2O$ (>99.0%), and 37% hydrogen peroxide were purchased from Sigma-Aldrich. All chemicals were used as received. Deionized water (DI) was used to dissolve the metal salts as described further.

Nanoparticle Synthesis. Noble metal nanoparticles were prepared with the modified citrate reduction method from Enustun et al.[31] In detail, for Au nanoparticles, we used 29 mL of a 0.2 wt % dihydrogen tetrachloroaureate hexahydrate aqueous solution stirring in a total volume of 500 mL of deionized water. Then 11.6 mL of a 1 wt % trisodium citrate solution was added, and after 30 s a subsequent injection of 5.8 mL containing 0.07 wt % sodium borohydride and 1 wt % trisodium citrate followed. The solution turns immediately from yellow to red. For Pt nanocrystals, a 1 L flask with 36.2 mL of an aqueous 0.2 wt % dihydrogen tetrachloroplatinate (IV) hexahydrate solution was added to a total volume of 500 mL of deionized water. The solution was stirred and heated until boiling. Then 11.6 mL of a 1 wt % trisodium citrate solution was added and stirred for 30 s to reach the boiling point again. Subsequently, 5.5 mL of an ice cold sodium borohydride solution with 0.076 wt % was added. The solution immediately changed from yellow to brown color. Ag nanocrystals were prepared similarly using 12 mL of an aqueous 0.2 wt % silver nitrate solution as noble metal precursor. When adding sodium borohydride, the solution changed from colorless to yellow.

Hematite nanoparticles were synthesized following the method described by Faust et al.[32] First, 150 mL of a 0.1 M iron(III) chloride hexahydrate solution was added dropwise into 600 mL of boiling water under stirring. The solution turned red immediately and was boiled under reflux for further 5 min. The solution was then dialyzed (dialyze tubes Medicell International, MWCO 12−14000 Da) for 3 days, with the tubes placed inside the distilled water, and was changed around 6−8 times.

Metal oxide hydroxide nanoparticles were synthesized following a modified synthesis route described by Deng et al.[33] by preparing a 1 wt % precursor solution of the corresponding metal(II) chlorides ($MnCl_2{\cdot}4H_2O$; $CoCl_2{\cdot}6H_2O$; $NiCl_2{\cdot}6H_2O$). To 10 mL of the precursor solution, 12 mL of a 1 wt % trisodium citrate solution was added and heated to 50 °C until the solution became colored (formation of metal complexes). From this solution, the metal oxide hydroxide nanoparticles were precipitated using a calculated volume (47 μL for the $MnCl_2$ solution and 167 μL for the $CoCl_2$ and $NiCl_2$ solution) of a mixture of 1 g of sodium hydroxide carefully dissolved in 5 mL of 37% hydrogen peroxide.

Ligand exchanges were performed by adding 0.33 mmol DMAT per mL of a 0.011 M Pt nanoparticle solution and letting the solution stir for 4 h at 40 °C. The solution was washed three times with a 10-fold volume of DI water over a centrifuge filter (Amicon Ultra-15, 10 kDa, Merck Millipore).

Cryoaerogel Synthesis. The cryoaerogels were synthesized following a modified synthesis route from Freytag et al.[21] To achieve volume fractions of nanoparticles of 0.1% or higher, we concentrated the colloidal solution of the single nanoparticles. Noble metal solutions were concentrated by a factor of 1000, hematite by a factor of 100, which equals a final volume fraction of 0.1 vol % of nanoparticles. Concentration of the colloidal solutions was achieved by an ultrafiltration cell (solvent resistant filtration cell, Merck Millipore) with a pressure of 5.5 bar filtering over a regenerated cellulose membrane (10 kDaA, Satorius Stedim) and subsequent filtration via ultrafiltration centrifuge filters (Amicon Ultra-15, 10 kDa, Merck Millipore) in a centrifuge at 3800 rcf for 10 min. The concentrated colloidal solutions were mixed according to the intended and calculated compound composition (0 wt %, 1 wt %, 50 wt %, 84 wt %, 100 wt %) and subsequently added dropwise into liquid nitrogen to obtain monoliths, or knife bladed on washed FTO glass substrates and subsequently dipped in liquid nitrogen to obtain cryoaerogel films. After freezing for approximately 5 min, the monolith and film samples were brought into a freeze-dryer (Christ, Alpha LD 1−2) and kept under vacuum (<0.05 mbar) for 24 h (monoliths) or 6 h (films).

Characterization. UV−vis absorption spectra of mixed TiO_2 noble-metal cryoaerogels immobilized on the FTO glass substrate were recorded using a slide holder and the spectrophotometer Cary 5000 (Agilent Technologies). Scattering free absorption measurements were carried out in the same spectrophotometer equipped with an integrating sphere (Agilent DRA 2500) measuring the films in center mount position. Scanning electron microscopy (SEM) was performed using a JEOL JFM 6700F electron microscope operated at 2 kV. The samples were prepared by placing small aerogel pieces onto an adhesive carbon polymer pad. Energy dispersive X-ray spectroscopy (EDX) measurements were carried out in the same device operated at 10 kV using a EDX detector (Oxford Instruments INCA 300). Transmission electron microscopy (TEM) was performed by a FEI Tecnai G2 F20 electron microscope, operated at 200 kV. The samples were prepared by pressing a carbon film coated copper mesh (mesh width 300 μm, Quanitfoil) gently onto the monolith or film. The particle size was (additionally to TEM imaging) determined using dynamic light scattering (DLS). For this measurement, a cuvette was filled with 3 mL of colloid and directly measured (Zetasizer ZSP, Malvern Instruments). ζ-Potentials were measured using a disposable folded capillary cell (DTS 1070, Malvern) within the Zetasizer ZSP. X-ray diffraction (XRD) patterns of the samples were measured using a Bruker D8 Advance in reflection mode. Highly concentrated samples of pristine metal nanoparticles were drop casted on a single crystal silicon carrier and were dried under ambient conditions. The solid samples were fixed with grease on the crystal silicon carrier. Krypton physisorption was performed at a Autosorb-1 instrument from Quantachrome operating at 87 K. Prior to physisorption measurements, the samples were degassed under vacuum at 100 °C for 24 h. Surface areas were estimated by applying the Brunauer−Emmett−Teller (BET) equation.

The content of noble metal or metal oxide in the cryoaerogels was determined within colloidal solution prior to cryoaerogelation (atomic absorption spectroscopy, AAS) for the noble metals. TiO_2 was used as received and dispersed in the solution. The colloidal stability was confirmed by DLS measurements to rule out possible sedimentation. Since all content was associated with the cryoaerogels after gelation, it can be inferred that the content in the gels was similar. This was further confirmed in the cryoaerogels by EDX-REM spectroscopy.

Photocatalysis Measurements. For photocatalysis measurements, 25 mg of the respective cryoaerogel monolith with varying composition (0 wt %, 1 wt %, 50 wt %, 84 wt %, 100 wt %) was redispersed in 10 vol % aqueous methanol (Roth, 99%) solution (photocatalyst concentration 0.5 g L^{-1}, initial suspension volume 50 mL, irradiation time 4 h, irradiation intensity $I_{250} - I_{450}$ 30 mW cm^{-2}). A continuous double jacket quartz glass reactor attached to a quadruple mass spectrometer (QMS (Hiden HPR-20)) was used to

DOI: 10.1021/acsanm.8b01333
ACS Appl. Nano Mater. 2018, 1, 6123−6130

carry out the photocatalytic test reactions. Argon (Ar) was used as a carrier gas with a constant flow rate of 10 mL/min. To maintain the temperature of photocatalytic reaction, a thermostat was used at 20 °C. For the removal of dissolved molecular oxygen, Ar was purged into the suspension for 30 min. Later on, the reactor was closed and flow of Ar gas was continued for 60 min until no traces of any other gas could be detected by QMS. Once the stabilization of the system was achieved, the lamp was switched on and illumination continued for 4 h. An Osram XBO 1000 W Xenon Arc Lamp in Müller LAX 1000 lamp housing was used as a light source. A sudden increase in the production rate for molecular hydrogen was detected immediately after the start of illumination. After 4 h of illumination, as the lamp was switched off, and a decrease in the production rate for molecular hydrogen was observed. The advantage of using this system is that the time course for the reaction products can be monitored during the photocatalytic experiments. The details of QMS setup are described by Kandiel et al.[30]

■ ASSOCIATED CONTENT

Supporting Information

The Supporting Information is available free of charge on the ACS Publications website at DOI: 10.1021/acsanm.8b01333.

Photographs of various cryogelated aerogel monoliths from mixed systems, TEM images of system TiO_2−Pt prepared from solution and from cryoaerogel, dynamic light scattering of nanoparticle solutions, EDX mappings from SEM, normalized absorption spectra of TiO_2-Ag cryoaerogel films, Krypton-physisorption measurements of noble metal−titania cryoaerogels, X-ray diffractograms of Pt, Au, and Ag nanoparticles, titania nanoparticles, and of respectively mixed cryoaerogels (PDF)

■ AUTHOR INFORMATION

Corresponding Author

*E-mail: nadja.bigall@pci.uni-hannover.de.

ORCID

Saher Hamid: 0000-0003-1594-9991

Detlef Bahnemann: 0000-0001-6064-6653

Nadja C. Bigall: 0000-0003-0171-1106

Funding

Financial support from the German Federal Ministry of Education and Research (BMBF) within the framework of NanoMatFutur, support code 03X5525. Furthermore, the project leading to these results has in part received funding from the European Research Council (ERC) under the European Unionś Horizon 2020 research and innovation program (Grant Agreement No. 714429).

Notes

The authors declare no competing financial interest.

■ ACKNOWLEDGMENTS

The authors thank A. Feldhoff and J. Caro for access to SEM and XRD, M. Jahns and P. Behrens for the Krypton-physisorption measurements, and D. Dorfs for discussion.

■ REFERENCES

(1) Huesing, N.; Schubert, U. Aerogels—Airy Materials: Chemistry, Structure, and Properties. *Angew. Chem., Int. Ed.* **1998**, *37*, 22−45.

(2) Mohanan, J. L.; Arachchige, I. U.; Brock, S. L. Porous Semiconductor Chalcogenide Aerogels. *Science* **2005**, *307*, 397−400.

(3) Koebel, M.; Rigacci, A.; Achard, P. Aerogel-Based Thermal Superinsulation: an Overview. *J. Sol-Gel Sci. Technol.* **2012**, *63*, 315−339.

(4) Elsila, J. E.; Glavin, D. P.; Dworkin, J. P. Cometary Glycine Detected in Samples Returned by Stardust Meteoritics & Planetary. *Meteorit. Planet. Sci.* **2009**, *44*, 1323−1330.

(5) Bigall, N. C.; Herrmann, A.-K.; Vogel, M.; Rose, M.; Simon, P.; Carrillo-Cabrera, W.; Dorfs, D.; Kaskel, S.; Gaponik, N.; Eychmueller, A. Hydrogels and Aerogels from Noble Metal Nanoparticles. *Angew. Chem., Int. Ed.* **2009**, *48*, 9731−9734.

(6) Heiligtag, F. J.; Rossell, M. D.; Sueess, M. J.; Niederberger, M. Template-Free Co-Assembly of Preformed Au and TiO_2 Nanoparticles into Multicomponent 3D Aerogels. *J. Mater. Chem.* **2011**, *21*, 16893−16899.

(7) Sánchez-Paradinas, S.; Dorfs, D.; Friebe, S.; Freytag, A.; Wolf, A.; Bigall, N. C. Aerogels from CdSe/CdS Nanorods with Ultra-long Exciton Lifetimes and High Fluorescence Quantum Yields. *Adv. Mater.* **2015**, *27*, 6152−6156.

(8) Naskar, S.; Schlosser, A.; Miethe, J. F.; Steinbach, F.; Feldhoff, A.; et al. Bigall Site-Selective Noble Metal Growth on CdSe Nanoplatelets. *Chem. Mater.* **2015**, *27*, 3159−3166.

(9) Bigall, N. C.; Haertling, T.; Klose, M.; Simon, P.; Eng, L. M.; Eychmueller, A. Monodisperse Platinum Nanospheres with Adjustable Diameters from 10 to 100 nm: Synthesis and Distinct Optical Properties. *Nano Lett.* **2008**, *8*, 4588−4592.

(10) Dorfs, D.; Hartling, T.; Miszta, K.; Bigall, N. C.; Kim, M. R.; Genovese, A.; Falqui, A.; Povia, M.; Manna, L. Reversible Tunability of the Near-Infrared Valence Band Plasmon Resonance in Cu(2-x)Se Nanocrystals. *J. Am. Chem. Soc.* **2011**, *133*, 11175−11180.

(11) Hinrichs, D.; Galchenko, M.; Kodanek, T.; Naskar, S.; Bigall, N. C.; Dorfs, D. Chloride Ion Mediated Synthesis of Metal/Semiconductor Hybrid Nanomaterials. *Small* **2016**, *12*, 2588−2594.

(12) Dorfs, D.; Salant, A.; Popov, I.; Banin, U. ZnSe Quantum Dots Within CdS Nanorods: A Seeded-Growth Type-II System. *Small* **2008**, *4*, 1319−1323.

(13) da Silva, R. O.; Heiligtag, F. J.; Karnahl, M.; Junge, H.; Niederberger, M.; Wohlrab, S. Design of Multicomponent Aerogels and their Performance in Photocatalytic Hydrogen Production. *Catal. Today* **2015**, *246*, 101−107.

(14) Freytag, A.; Colombo, M.; Bigall, N. C. Catalytic Properties of Cryogelated Noble Metal Aerogels. *Z. Phys. Chem.* **2017**, *231*, 63−75.

(15) Munnik, P.; de Jongh, P. E.; de Jong, K. P. Recent Developments in the Synthesis of Supported Catalysts. *Chem. Rev.* **2015**, *115*, 6687−6718.

(16) Wang, C.; Liu, R.; Zhang, W.; Wang, Y.; Xu, K.; Yue, Z.; Liu, G. Multichannel Scan Surface Plasmon Resonance Biochip with Stationary Optics and Baseline Updating Capability. *J. Biomed. Opt.* **2013**, *18*, 115002.

(17) Liu, W.; Rodriguez, P.; Borchardt, L.; Foelske, A.; Yuan, J.; Herrmann, A.-K.; Geiger, D.; Zheng, Z.; Kaskel, S.; Gaponik, N.; Koetz, R.; Schmidt, T. J.; Eychmueller, A. Bimetallic Aerogels: High-Performance Electrocatalysts for the Oxygen Reduction Reaction. *Angew. Chem., Int. Ed.* **2013**, *52*, 9849−9852.

(18) Pajonk, G. M. Catalytic Aerogels. *Catal. Today* **1997**, *35*, 319−337.

(19) Heiligtag, F. J.; Kranzlin, N.; Suess, M. J.; Niederberger, M. Anatase−Silica Composite Aerogels: a Nanoparticle-Based Approach. *J. Sol-Gel Sci. Technol.* **2014**, *70*, 300−306.

(20) Fricke, J.; Emmerling, A. Aerogels. *J. Am. Ceram. Soc.* **1992**, *75*, 2027−2035.

(21) Freytag, A.; Sanchez-Paradinas, S.; Naskar, S.; Wendt, N.; Colombo, M.; Pugliese, G.; Poppe, J.; Demirci, C.; Kretschmer, I.; Bahnemann, D. W.; Behrens, P.; Bigall, N. C. Versatile Aerogel Fabrication by Freezing and Subsequent Freeze-Drying of Colloidal Nanoparticle Solutions. *Angew. Chem., Int. Ed.* **2016**, *55*, 1200−1203.

(22) Geguzin, J. E. *Physik des Sinterns*; VEB Deutscher Verlag für Grundstoffindustrie: Leipzig, 1973.

(23) von Smoluchowski, M. Studies on Colloid Statistics and Mechanism of Diffusion M. *Colloid Polym. Sci.* **1916**, *18*, 48−54.

(24) Smoluchowski, M. Mathematical theory of the kinetics of the coagulation of colloidal solutions. *Z. Phys. Chem.* **1917**, *92*, 129−68.

DOI: 10.1021/acsanm.8b01333
ACS Appl. Nano Mater. 2018, 1, 6123−6130

(25) Kaise, M.; Nagai, H.; Tokuhashi, K.; Kondo, S.; Nimura, S.; Kikuchi, O. Electron-Spin-Resonance Studies of Photocatalytic Interface Reactions of Suspended M/TiO(2) (M = Pt, Pd, Ir, Rh, Os, Or Ru) with Alcohol and Acetic-Acid in Aqueous-Media. *Langmuir* **1994**, *10*, 1345−1347.
(26) Haertling, T.; Alaverdyan, Y.; Hille, A.; Wenzel, M. T.; Kaell, M.; Eng, L. M. Optically Controlled Interparticle Distance Tuning and Welding of Single Gold Nanoparticle Pairs by Photochemical Metal Deposition. *Opt. Express* **2008**, *16*, 12362−12371.
(27) Kodanek, T.; Freytag, A.; Schlosser, A.; Naskar, S.; Härtling, T.; Dorfs, D.; Bigall, N. C. Macroscopic Aerogels with Retained Nanoscopic Plasmonic Properties. *Z. Phys. Chem.* **2018**, *232*, 1675−1689.
(28) Haertling, T.; Alaverdyan, Y.; Hille, A.; Wenzel, M. T.; Kaell, M.; Eng, L. M. Optically Controlled Interparticle Distance Tuning and Welding of Single Gold Nanoparticle Pairs by Photochemical Metal Deposition. *Opt. Express* **2008**, *16*, 12362−12371.
(29) Sönnichsen, C.; Reinhard, B. M.; Liphardt, J.; Alivisatos, A. P. A Molecular Ruler Based on Plasmon Coupling of Single Gold and Silver Nanoparticles. *Nat. Biotechnol.* **2005**, *23*, 741−5.
(30) Kandiel, T. A.; Ivanova, I.; Bahnemann, D. W. Long-term Investigation of the Photocatalytic Hydrogen Production on Platinized TiO_2: An Isotopic Study. *Energy Environ. Sci.* **2014**, *7*, 1420−1425.
(31) Enustun, B. V.; Turkevich, J. Coagulation of Colloidal Gold. *J. Am. Chem. Soc.* **1963**, *85*, 3317−28.
(32) Faust, B. C.; Hoffmann, M. R.; Bahnemann, D. W. Photocatalytic Oxidation of Sulfur Dioxide in Aqueous Suspensions of.Alpha.-Iron Oxide (Fe2O3). *J. Phys. Chem.* **1989**, *93*, 6371−6381.
(33) Deng, X.-Y.; Xiang, L.; Jin, Y. Preparation of NiO nanoparticles via liquid chemical precipitation. *Harbin Gongye Daxue Xuebao* **2002**, *34*, 214−216.

DOI: 10.1021/acsanm.8b01333
ACS Appl. Nano Mater. 2018, 1, 6123−6130